UAS-SfM versus TLS: Vertical Error Assessment on a Wetland

José A. Pilartes-Congo

ABSTRACT

This experiment compares two specific remote sensing modalities for point cloud generation over coastal wetlands: an uncrewed aircraft system (UAS)-based photogrammetry, and a terrestrial laser scanning (TLS) system. Assessments include comparing differences in vertical error statistics, point density variability, and the quality of derived geospatial data products. Results show that TLS denser point clouds but the spatial distribution of those degrade over larger distances, and quality is affected by occlusion and distance related errors, particularly when using singular scan positions. In contrast, UAS-based photogrammetry offers broader spatial coverage and more uniform point distribution but lacks vertical precision in some complex surfaces. Results further highlight the influence of perspective sensing differences on relative comparison between the two systems.

INTRODUCTION

Close-range photogrammetry (CRP) and light detection and ranging (lidar) scanning modalities support repeat, rapid, and cost-effective wetland monitoring at small geographic scales, further enhanced by their ability to perform or conduct field measurements with minimal ecosystem disturbance [1–3]. In this context, two commonly used data collection modes include uncrewed aircraft system (UAS)-based structure-from-motion / multi-view stereo photogrammetry (UAS-SfM) and lidar-based terrestrial laser scanning (TLS), each with distinct strengths, limitations, and environment sensing principles that influence their utility for monitoring complex environments such as coastal wetlands.

UAS-SfM is a passive data sensing technique that reconstructs three-dimensional (3D) surface or object geometries using common features (or keypoints) in overlapping two-dimensional (2D) imagery, aided by advanced computer vision algorithms [4-7]. UAS-SfM is known for its cost-effectiveness and ease of use in collecting high resolution geospatial data, including 3D point clouds, orthomosaic, and digital elevation models (DEMs), which in turn can be used for tasks such as topographic monitoring and surface change detection [5,7,8]. As an aerial sensing technology, UAS-SfM provides broad area coverage with uniform spatial sampling, which supports survey missions over larger areas [8]. However, UAS-SfM is sensitive to ambient lighting conditions, vegetation motion and density, as well as surface texture, all of which limit its mapping usefulness in topographic modeling of natural environments [3,9,10]. In comparison, TLS is an active laser scanning method that creates 3D point clouds by emitting laser pulses onto a surface and measuring the two-way travel time it takes for them to return [3,11,12]. TLSs are particularly effective in resolving vertical structures and some related sensors are able to penetrate canopy cover, enhancing its ability to map the terrain beneath vegetation [3]. While TLS is less affected by lighting or surface reflectance and offers high geometric fidelity, its deployment in wetland mapping is limited to a ground perspective, which can lead to occlusions, incomplete data, and reduced spatial coverage, which can lead to reduced densities, particularly in areas obstructed by terrain or tall vegetation. Terrain stability also limits TLS use, often prompting multiple scan stations for complete data collection, which could lead to time-consuming fieldwork workflows and added labor expenses [13].

The applicability of UAS-SfM for mapping or monitoring wetlands has been widely discussed in the literature, including uses in general wetland mapping, [14], delineation and classification of wetlands and related land covers [14,15], wetland restoration [16], botanical species identification [17], and others. Similarly, TLS has been used in tasks such as automated wetland segmentation and land cover type classification [2], biomass estimation [18], microtopography quantification [19], marsh edge erosion and restoration [20], and assessment of vegetation structure [21]. These applications underscore the need for continuous and comparative analyses of UAS-SfM and TLS

sensors as well as error budgets when deployed under consistent environmental conditions. This prompts the following research question: How does the nature of UAS-SfM and TLS data acquisition affect 3D point cloud density, vertical accuracy, data quality in wetland mapping? To address this question, this experiment compares point clouds derived from specific UAS-SfM and TLS systems over the same test site.

The experiment provides the following key contributions: (1) assessment of point density and its spatial variability across the study area, (2) evaluation of absolute and relative vertical accuracy, and (3) development of an automated, scalable technique for rapid comparison of point cloud data. These assessments support effective and informed deployment of UAS-SfM and TLS in coastal wetland topographic mapping.

MATERIALS & METHODS

Study Area and Data Sets

This experiment uses point cloud data acquired over a coastal wetland area located on the back side of Mustang Island Observatory (Figure 1), Texas. The test site is characterized by a variety of land covers such as exposed tidal flats, a gravel roadway, short and tall grass, and mangroves [3]. This mixture of land covers make it ideal for assessing UAS-SfM and TLS performance under realistic field conditions. The data was provided by Dr. Michael J. Starek of the Measurement Analytics Lab (MANTIS).

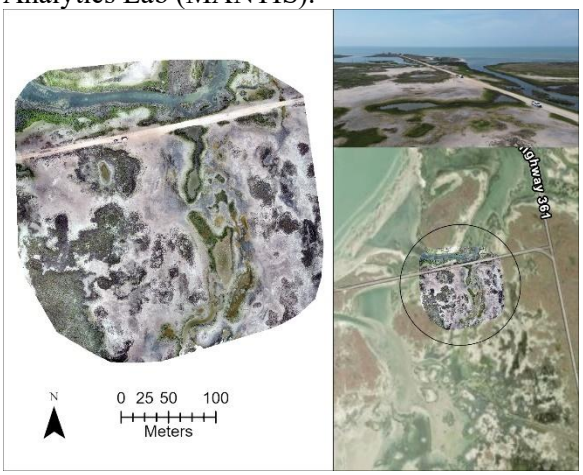

Figure 1. Mustang Island Observatory test site

The data was acquired on March 14, 2017, using a DJI Phantom 4 and a TLS mounted on a tripod. The DJI is a rotary-wing UAS platform equipped with a consumer-grade, 12.4-megapixel digital camera. The TLS system encompassed a RIEGL VZ-400 lidar scanner and a digital camera for point cloud colorization. The scanner operates in the near-infrared band and has multi-return laser capabilities. Ground truth data consisted of 72 observations collected using real-kinematic (RTK) global navigation satellite system (GNSS) on January 23, 2017. Due to logistical constraints, the survey team was unable to collect ground truth data on the same day as the UAS and TLS surveys. More discussion about the datasets used and sensors deployed is available in [2].

Methods

The first step in this experiment was to retrieve the datasets from MANTIS. Next, point cloud statistics were obtained using the *lasinfo* module of LAStools, which provided general point cloud information such as the total number of points. Point cloud density was retrieved using the *laspy* library for processing point cloud data, *lasgrid* was used to map the spatial distribution of the points, using primarily a grid resolution of 50 cm. However, examples of 1 m gridding were also generated for comparison purposes.

The absolute accuracy of the point clouds was examined using *lascontrol* as well as the *KDTree* Python module of the *scikit-learn* library. Since both provided similar metrics, the latter was used in this report as it provided helpful estimates that are not available in *lascontrol* by default. Also, to ensure a fair comparison and minimize the effects of different viewpoints between the sensors, the original data was clipped to a common (via *lasclip*) using a shapefile buffer of 60 meters centered on the TLS scan position (Appendix 1). The buffer was created in ArcGIS Pro. Figure 2 shows the resulting data. Appendix 2 and Appendix 3 show the extent of the original point clouds before the clipping operation.

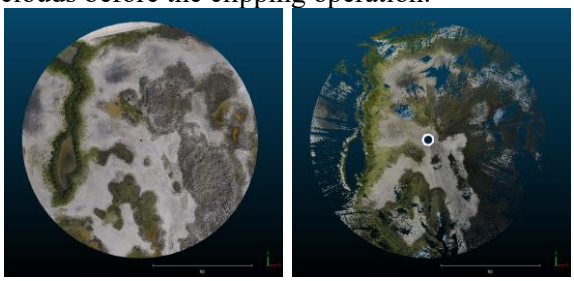

Figure 2. Clipped SfM (right) and TLS (left) point clouds.

Point cloud noise filtering and classification was performed using *lasnoise* and *lasclassify*. DEMs were generated using *blast2dem* and a spatial resolution of 50 cm (Appendix 4 and Appendix 5). The DEMs were then used to create a DEM of Differences (DoD) map, via the Raster Calculator tool in ArcGIS Pro. In this case, the TLS point cloud was set as the reference dataset (i.e., SfM - TLS). DoD statistics were retrieved (using both the statistics summary option in ArcGIS Pro and the *rasterio* Python library), root mean square error (RMSE), standard deviation, average error, and maximum/minimum metrics. Next, using CloudCompare, a cloud-to-cloud (C2C) valuation was performed. C2C is used to quantify the geometric difference between point clouds [23. Here, the TLS point cloud was set as the reference again (see Appendix 6). The result included metrics such as the minimum and maximum distance, the average distance, the standard deviation, and the maximum error.

Finally, qualitative evaluation was performed based on shaded relief maps and side-by-side visualizations of the point clouds to assess dataset completeness and overall quality in representing the mapped area. ArcGIS Pro and Python were used for map creation and visualization. All data products were georeferenced to North American Datum of 1983 (2011), and orthometric heights converted from the ellipsoid using GEOID 12B. All LAStools operations were conducted using the 64-bit executable files due to memory challenges posed by the 32-bit versions. The various LAStools commands used are shown in Appendix B – Control Commands. The Python code that supported this experiment is available via https://github.com/jpilartescongo/misc. Note that AI was used to support parts of this work.

RESULTS

Assessments Using Original Point Cloud

Point cloud statistics assessments yielded a total of 46,826,521 points for the original UAS-SfM (henceforth referred to as SfM) point cloud, and 37,672,780 points for TLS point cloud. Table 1 summarizes the total number of points per sensor as well as their respective distributions according to level of return. Figure 3 illustrates the spatial variability of UAS-SfM point density, and Figure 4 shows the density distribution of the TLS point cloud across the survey site. As shown, SfM yielded a more consistent density throughout the area, but the TLS observed higher point densities, although mostly concentrated around the scanner position, with the density decreasing radially as the distance increased.

Table 1. General point cloud statistics

	$SfM_{original}$	$TLS_{original}$
N. of points (total)	46,826,521	37,672,780
No. of first returns	0	35,740,440
No. of middle returns	46,826,521	529,673
No. of last returns	46,826,521	35,740,440
No. of single returns	46,826,521	34,337,773
Never classified	46,826,521	37,672,780

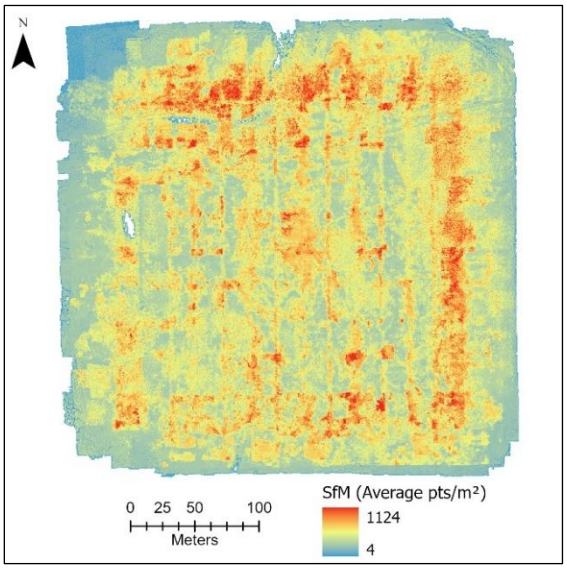

Figure 3. SfM density map (50 cm resolution).

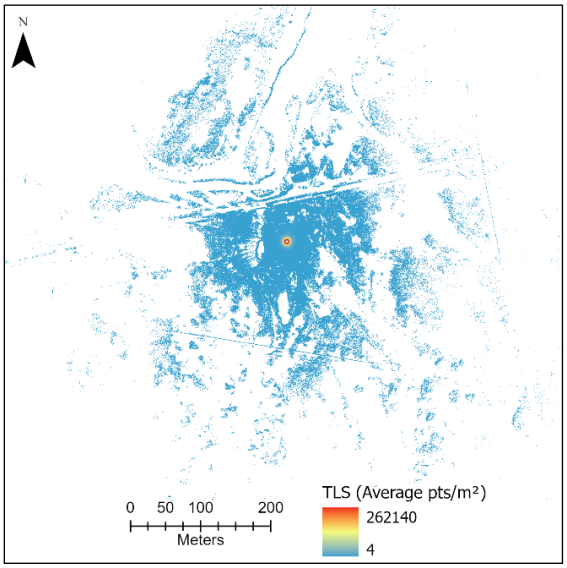

Figure 4. TLS density map (50 cm resolution).

Accuracy assessment results (Figure 5) suggest that lower overall errors were obtained with SfM compared to TLS. SfM observed an RMSE of 0.0716 m, standard deviation of 0.0561 m, and mean error of 0.0446 m compared to an RMSE of 0.2484 m, standard deviation of 0.1829 m, and mean error of 0.1676 m for TLS. The median and mean absolute error (MAE) values for TLS are 0.0944 m and 0.1697 m, respectively (versus 0.0367 m and 0.0534 m, respectively for SfM), which suggest greater vertical discrepancies in TLS measurements across the area.

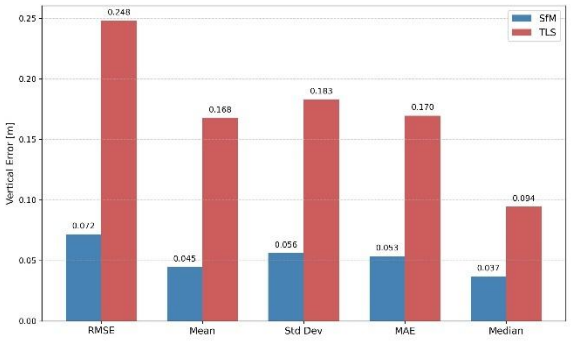

Figure 5. Absolute accuracy metrics.

Relative Assessments (Common Area)

Table 2 summarizes point cloud statistics for the clipped point cloud datasets, each covering an area of nearly 4,060 m^2. SfM observed 4,575,513 points and an average of 325.20 points p/m^2. In contrast, the TLS resulted in 35,409,031 points and a 2,518.08 pts/m^2 average point density. Table 3 summarizes DEM differencing (DoD) metrics (SfM minus TLS), and Figure 6 shows a map of elevation differences throughout the area.

Table 2. General point cloud statistics after clipping.

	$SfM_{clipped}$	$TLS_{clipped}$
N. of points (total)	4,575,513	35,409,031
No. of first returns	0	34,512,164
No. of middle returns	4,575,513	149,090
No. of last returns	4,575,513	34,451,836
No. of single returns	4,575,513	33,704,059
Never classified	4,575,513	35,409,031

Table 3. DEM of difference statistic metrics.

	Value
RMSE (m)	0.241
Standard deviation (m)	0.221
Mean (m)	-0.096
Average error (m)	0.106
Median (m)	0.637
Minimum (m)	-33.484
Maximum (m)	0.063

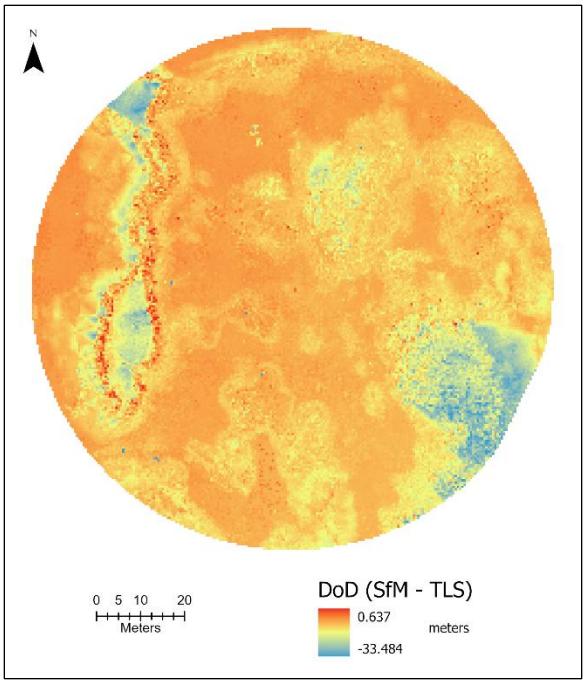

Figure 6. DEM of differences (5 cm resolution).

As shown, this differencing step led to an RMSE of 0.241 m, a standard deviation of 0.221 m, a mean value of -0.096 m, an average error of 0.106 m, median of 0.637 m, and minimum and maximum values of -33.484 m and 0.063 m, respectively. The minimum and maximum values, specifically, highlight areas where the highest elevation differences between the two sensors occurs. In Figure 6, these are the water surfaces (blue) and taller vegetated features (red). Finally, C2C results (Table 4) yielded an average point distance of 0.198 m, and a standard deviation of 0.594 m. Further, the minimum and maximum distance values observed were 0.000 m and 7.479 m respectively, with a maximum error of 0.464 m. These are summarized in Table 4.

Table 4. Cloud-2-cloud Results.

	Value
Average distance (m)	0.198
Standard deviation (m)	0.594
Minimum distance (m)	0.000
Maximum distance (m)	7.479
Maximum error (m)	0.464

Qualitative Assessment

Grid resolution tests stressed the importance of using the appropriate resolution for visualization purposes, especially if using the derived products to communicate important information. These are

well exemplified by Appendix 7 and Appendix 8, where the 50 cm map captures spatial detail with greater resolvability its 1 m counterpart. This is particularly relevant when using these sensors for assessing not just the quality but also the completeness of data product reconstruction.

The aerial versus ground perspective also plays a central role in effective product visualization and result communication. For example, Figure 7 and Figure 8 emphasize that the nadir perspective (i.e., SfM) helps to better distinguish between different features (e.g., GCP targets) while top-down visualization of TLS data is hindered by occlusions, shadowing, and leads to incomplete surface representation. In contrast, and as shown in Appendix 9 and Appendix 10, SfM models vertical structures in a flat manner, with poor volumetric definition and vertical completeness, whereas TLS represents vertical structure better.

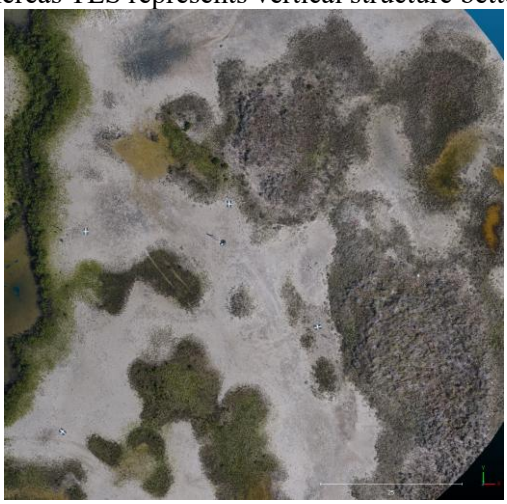

Figure 7. Aerial perspective (SfM).

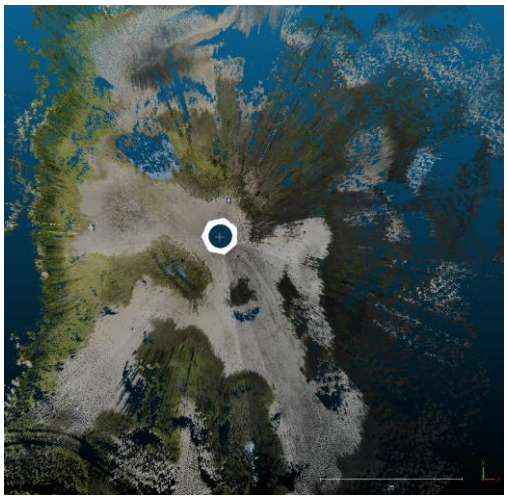

Figure 8. Aerial perspective (TLS).

DISCUSSION

Absolute Accuracy

Absolute errors relative to RTK GNSS yielded better results for SfM (at least in the evaluated context). The lower RMSE obtained with SfM suggest minimal deviation of measurements from the mean. TLS, in contrast, was less accurate, likely because of decreased density in areas far from the scanner, potential occlusion due to vegetation, similar to observations made in [2]. Multiple scan positions could have helped to prevent this issue. In addition, since the ground truth data used for this assessment is from a different date, it is likely that seasonal variation may also have a negative impact on these results, especially considering that vegetation growth in the TLS scan might have been more accentuated since it was summer season, while the ground truth data is from the winter. This would likely affect the SfM accuracy as well but potentially to a lesser degree because SfM was more uniform in point cloud generation and distribution through the scene. The density aspect of these effects were observed when using *lascontrol* to evaluate accuracy metrics, which at times caused the TLS not to have enough points around certain checkpoints while SfM did not observe said issue. These challenges emphasize the importance of collecting ground truth data simultaneously with data collection campaigns.

Relative accuracy assessments in a common area showed a much higher point density for TLS compared to SfM. DoD analysis highlighted differences in point clouds between the two sensors, likely caused by reasons such as the nature of data acquisition as well as systematic characteristics that affect both in different ways. The negative mean and relatively high standard deviation could be indicative of SfM struggles in modeling certain surfaces with the same level of performance as a TLS, which is expected in areas such as vegetation or surfaces with water. The high discrepancies (particularly the minimum value of -33.484 m) could result from differences in data scanning or sensing perspectives between the two systems, with the TLS more prone to occlusion given its ground-based perspective. Similarly, in water features, Figure 6 suggests that the SfM derived surface is lower than that of the TLS, which indicates that SfM underestimates

the elevation in that area (relative to the TLS). This could be because of motion-induced noise such as in water features which is a known, common limitation of SfM. Despite these differences, the two datasets show good agreement in flat, vegetation-free areas, which shows that either can effectively be used for mapping unobstructed areas.

C2C results show good spatial agreement between the two point clouds, which is indicated by the relatively low average distance (i.e., 0.198 m) and maximum error (0.464 m) values. This could be a result of accurate georeferencing of the two sets of data. However, the high maximum distance of 7.479 m could indicate challenges or noise in more complex areas such as vegetated sections of the test site.

CONCLUSIONS

This experiment evaluated specific SfM and TLS systems in terms of absolute and relative accuracy, and data product quality for wetland mapping. Results showed that SfM provides more consistent point cloud densities across the study area, outperforming TLS in terms of spatial completeness. While TLS offers attractive spatial resolutions and accurate representation of vertical structures, its effectiveness is constrained by limited perspective and occlusions. Despite these challenges being solvable by adding more scan positions to the field workflow, doing so could increase expenses and lead to more ecosystem disturbance. The results observed highlight the influence of sensor perspective on data quality, with SfM better suited for open, planar surfaces and TLS better for vertical features and surveying smaller areas. Future experiments could assess sensor integration for surface wetland mapping and surface change detection.

REFERENCES

[1] Turner, I.L., Harley, M.D. and Drummond, C.D., 2016. UAVs for coastal surveying. *Coastal Engineering*, 114, pp.19-24.

[2] Nguyen, C., Starek, M.J., Tissot, P. and Gibeaut, J., 2019. Unsupervised clustering of multi-perspective 3D point cloud data in marshes: a case study. *Remote Sensing*, 11(22), p.2715.

[3] Starek, M.J., Berryhill, J., Pashaei, M., Congo, J., Chu, T., Shukla, H. and Quiroga, C., 2024. Unmanned Aircraft Systems in Land Surveying: *A Comparative Study of Lidar and Photogrammetry* (No. FHWA/TX-25/0-7157-R1). Texas Department of Transportation. Research and Technology Implementation Office.

[4] Westoby, M.J., Brasington, J., Glasser, N.F., Hambrey, M.J. and Reynolds, J.M., 2012. 'Structure-from-Motion' photogrammetry: A low-cost, effective tool for geoscience applications. *Geomorphology*, 179, pp.300-314.

[5] Pilartes-Congo, J., Simpson, C., Starek, M.J., Berryhill, J., Parrish, C. and Slocum, R., 2024. Empirical Evaluation and Simulation of GNSS Solutions on UAS-SfM Accuracy for Shoreline Mapping. *Drones*, 8(11), p.646.

[6] Kholil, M., Ismanto, I. and Fu'Ad, M.N., 2021, February. 3D reconstruction using structure from motion (SFM) algorithm and multi view stereo (MVS) based on computer vision. In *IOP Conference Series: Materials Science and Engineering* (Vol. 1073, No. 1, p. 012066). IOP Publishing.

[7] Meinen, B.U. and Robinson, D.T., 2020. Mapping erosion and deposition in an agricultural landscape: Optimization of UAV image acquisition schemes for SfM-MVS. *Remote Sensing of Environment*, 239, p.111666.

[8] Sturdivant, E.J., Lentz, E., Thieler, E., Farris, A., Weber, K., Remsen, D.P., Miner, S. and Henderson, R.E., 2017. UAS-SfM for coastal research: Geomorphic feature extraction and land cover classification from high-resolution elevation and optical imagery. *Remote Sensing*, 9(10), p.1020.

[9] Berra, E.F. and Peppa, M.V., 2020, March. Advances and challenges of UAV SFM MVS photogrammetry and remote sensing: Short review. In 2020 IEEE Latin American GRSS & ISPRS Remote Sensing Conference (IAGIRS) (pp. 533-538). IEEE.

[10] Wallace, L., Lucieer, A., Malenovský, Z., Turner, D. and Vopěnka, P., 2016. Assessment of forest structure using two UAV techniques: A comparison of airborne laser scanning and structure from motion (SfM) point clouds. *Forests*, 7(3), p.62.

[11] Lemmens, M., 2011. Terrestrial laser scanning. In *Geo-information: technologies, applications and the environment* (pp. 101-121). Dordrecht: Springer Netherlands.

[12] Aryan, A., Bosché, F. and Tang, P., 2021. Planning for terrestrial laser scanning in construction: A review. *Automation in Construction*, 125, p.103551.

[13] Chen, J.L., Li, H.B., Jiang, N., Chen, Q., Yang, Y.C. and Zhou, J.W., 2025. Stability evaluation of shallow blocks in high and steep slope combining TLS and UAV photogrammetry. *Geomatics, Natural Hazards and Risk*, 16(1), p.2464052.

[14] Jeziorska, J., 2019. UAS for wetland mapping and hydrological modeling. *Remote Sensing*, 11(17), p.1997.

[15] Boon, M.A., Greenfield, R. and Tesfamichael, S., 2016. Wetland assessment using unmanned aerial vehicle (UAV) photogrammetry. The International Archives of the Photogrammetry, *Remote Sensing and Spatial Information Sciences*, 41, pp.781-788.

[16] Durgan, S.D., Zhang, C., Duecaster, A., Fourney, F. and Su, H., 2020. Unmanned aircraft system photogrammetry for mapping diverse vegetation species in a heterogeneous coastal wetland. *Wetlands*, 40(6), pp.2621-2633.

[17] Bertacchi, A., Giannini, V., Di Franco, C. and Silvestri, N., 2019. Using unmanned aerial vehicles for vegetation mapping and identification of botanical species in

wetlands. *Landscape and Ecological Engineering*, 15(2), pp.231-240.
[18] Owers, C.J., Rogers, K. and Woodroffe, C.D., 2018. Terrestrial laser scanning to quantify above-ground biomass of structurally complex coastal wetland vegetation. *Estuarine, Coastal and Shelf Science*, 204, pp.164-176.
[19] Stovall, A.E., Diamond, J.S., Slesak, R.A., McLaughlin, D.L. and Shugart, H., 2019. Quantifying wetland microtopography with terrestrial laser scanning. *Remote Sensing of Environment*, 232, p.111271.
[20] Huff, T.P., Feagin, R.A. and Delgado Jr, A., 2019. Understanding lateral marsh edge erosion with terrestrial laser scanning (TLS). *Remote Sensing*, 11(19), p.2208.
[21] Penman, S., Lentini, P., Law, B. and York, A., 2023. An instructional workflow for using terrestrial laser scanning (TLS) to quantify vegetation structure for wildlife studies. *Forest Ecology and Management*, 548, p.121405.
[22] Ahmad Fuad, N., Yusoff, A.R., Ismail, Z. and Majid, Z., 2018. Comparing the performance of point cloud registration methods for landslide monitoring using mobile laser scanning data. *The International Archives of the Photogrammetry, Remote Sensing and Spatial Information Sciences*, 42, pp.11-21.

APPENDICES

Appendix A – Supporting Images

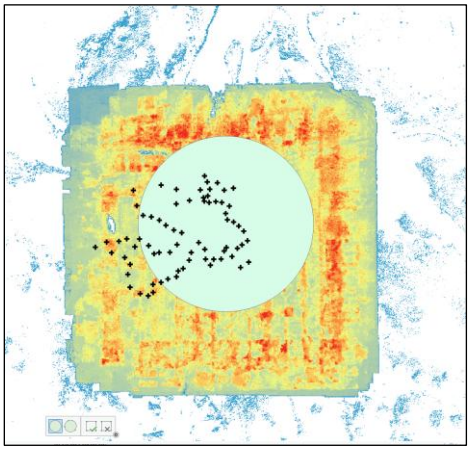

Appendix 1. Point cloud 60 m clipping buffer.

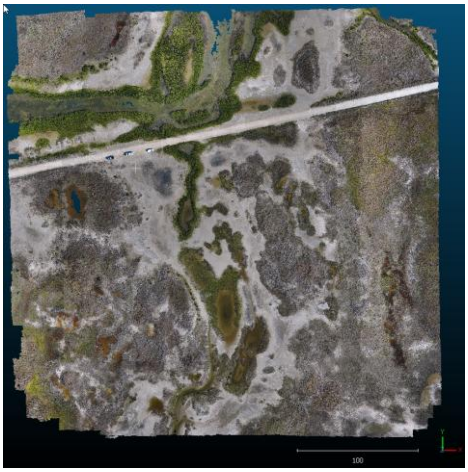

Appendix 2. Coverage extent of original SfM data.

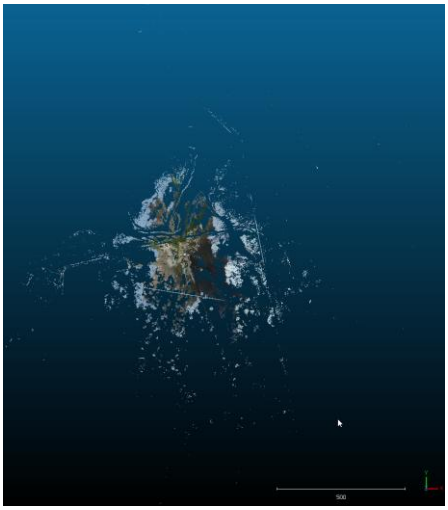

Appendix 3. Coverage extent of original TLS data.

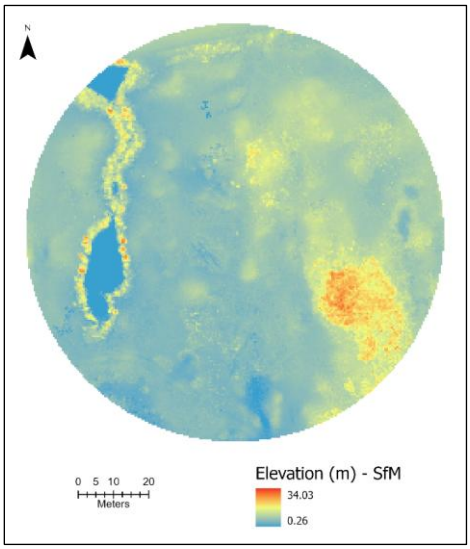

Appendix 4. SfM DEM (50 cm resolution).

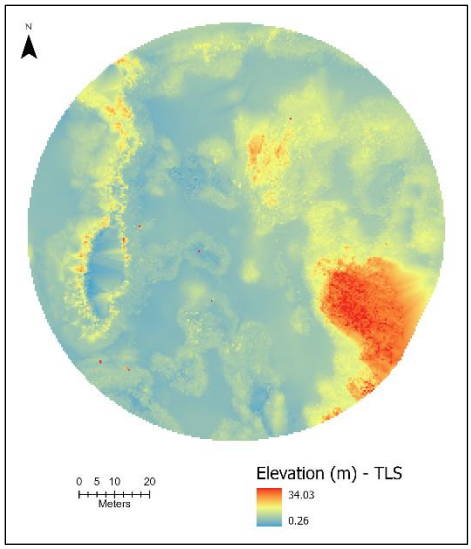

Appendix 5. TLS DEM (50 cm resolution).

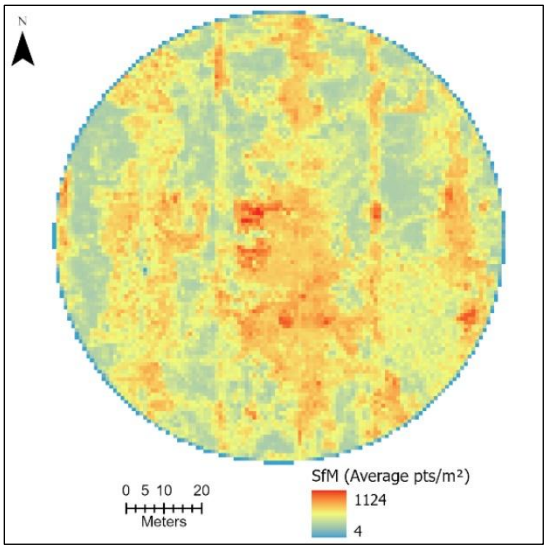

Appendix 8. SfM density (1 m grid resolution).

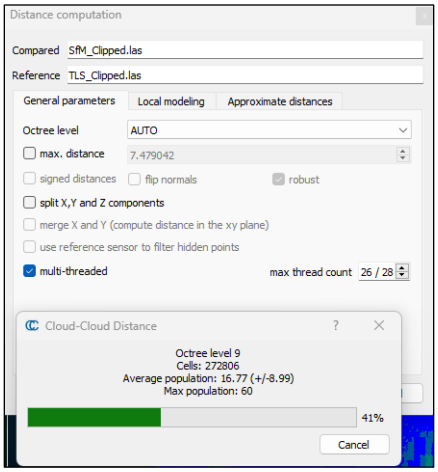

Appendix 6. C2C interface in CloudCompare during processing (using TLS point cloud as reference).

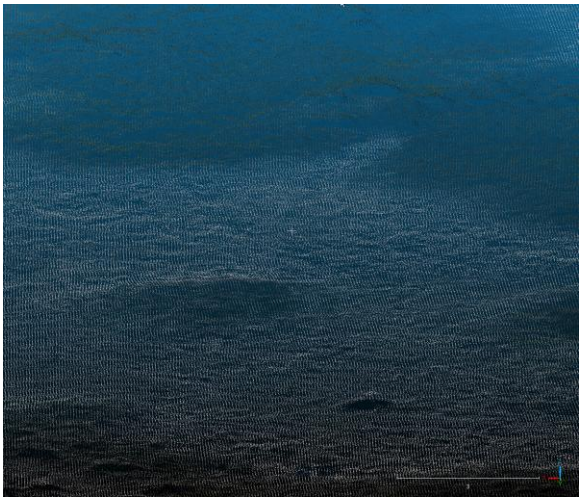

Appendix 9. Terrestrial perspective (SfM).

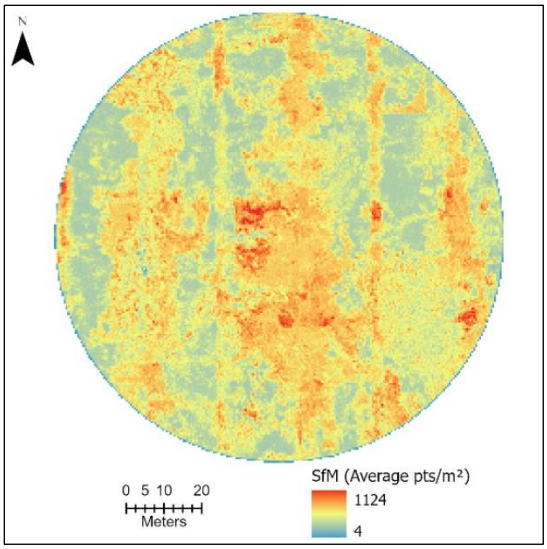

Appendix 7. SfM density (50 cm resolution).

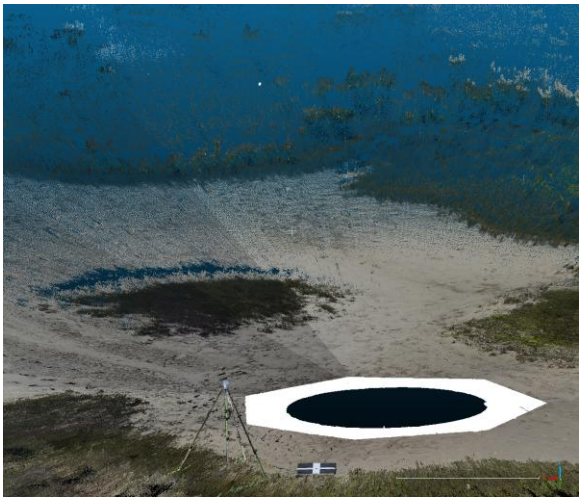

Appendix 10. Terrestrial perspective (TLS).

Appendix B – Control Commands

Clip:

lasclip -i SfM_3_14_2017_MUI.las -poly Circle.shp -o SfM_Clipped.las

lasclip -i TLS_3_14_2017_MUI.las -poly Circle.shp -o TLS_Clipped.las

Noise Filtering:

lasnoise64.exe -i SfM_Clipped.las -remove_noise -o SfM_Clipped_NoiseRemoved.las

lasnoise64.exe -i TLS_Clipped.las -remove_noise -o TLS_Clipped_NoiseRemoved.las

Ground Point Classification:

lasground_new64.exe -i SfM_Clipped_NoiseRemoved.las -step 1 -wilderness -o SfM_GroundClass.las

lasground_new64.exe -i TLS_Clipped_NoiseRemoved.las -step 1 -wilderness -o TLS_GroundClass.las

Point Cloud Classification:

lasclassify64.exe -i SfM_GroundClass.las -step 1 -small_trees

lasclassify64.exe -i TLS_GroundClass.las -step 1 -small_trees

blast2dem64.exe -i SfM_GroundClass_1.las -step 1 -elevation_meter -merged -nad83 -o SfM_DEM_1m.tif

blast2dem64.exe -i TLS_GroundClass_1.las -step 1 -elevation_meter -merged -nad83 -o TLS_DEM_1m.tif